Selective, Ultra-Sensitive, and Rapid Detection of Serotonin by Optimized ZnO Nanorod FET Biosensor

K. Sinha, B. Chakraborty, S. Som Chaudhury, C. Roy Chaudhuri, *Senior Member, IEEE*, S. K. Chattopadhyay, and C. Das Mukhopadhyay

***Abstract*— Background: Fluctuation in serotonin (5-HT) level is an essential manifestation of several neurological disorders. In view of such importance, it is necessary to monitor the levels of 5-HT with good sensitivity, selectivity, affordability and low response time. Zinc oxide (ZnO) based field effect transistors (FET) with attributes like minimized noise levels and large on-off ratio are regarded as emerging high performance biosensor platforms. However, their response is significantly non-linear and there has been no appreciable endeavor for improving the non-linearity. Method: In this paper, we have introduced embedded gate electrode encompassing the channel of the FET which improves the uniformity in electric field line distribution through the electrolyte and proportionately enhances the capture of target biomolecule at ultra-low concentrations, thereby increasing the linearity. Further, we have incorporated the optimized parameters of ZnO nanorods reported previously, for rapid and selective detection of 5-HT. Results: It has been observed that the fabricated ZnO FET biosensor lowers the detection limit down to 0.1fM which is at least one order of magnitude lower than the existing reports. The sensor also has wide linear range from 0.1fM to 1nM with a detection time of about 20 minutes. Conclusion: The proposed zinc oxide nanorod-based sensor can be used as an excellent tool for future diagnosis of neurological disorders.**

***Index Terms*— Serotonin, zinc oxide nanorod, neurological disorder, optimization.**

I. Introduction

MONITORING of serotonin (5-hydroxytryptamine, 5-HT) using biosensors is a potent research area because imbalanced 5-HT in blood causes depression, a major world-wide public health problem. [1]–[5]. Moreover, a low level of 5-HT can also lead to numerous abnormal physiological conditions like kidney disorder, regulation of blood pressure, hypertension, fibrotic syndrome and others [6]–[10]. Therefore, trace level detection of 5-HT is necessary for early diagnosis and prevention of various neurological diseases [11], [12]. Few basic criteria for large scale monitoring of 5-HT include good sensitivity, high selectivity, affordability, low response time and superior portability. Moreover, due to the complicated matrix of physiological analytes, it is highly challenging to develop a sensing strategy, which combines all the required criteria. For instance, the widely deployed laboratory based methods for 5-HT detection include high-performance liquid chromatography (HPLC), capillary electrophoresis, coulometry, fluorescence, mass spectrometry and enzyme-based immunoassay, which have good sensitivity as well as selectivity, but require sophisticated instrumentation and tedious sample pre-treatment, in addition to being time consuming [13]–[17]. Various electrochemical techniques have also been deployed for precise detection of 5-HT, because they are simple, economical and enable rapid, label free detection in a real-time manner [18], [19]. Despite, these advantageous features, it is often difficult for electrochemical based methods to achieve high selectivity towards the target molecule, especially in case of neurotransmitters because the oxidation potential of these small molecules are significantly close and is often difficult to differentiate their electrical signals [20].

Recent evidences suggest that immunoassays are highly advantageous for specific and sensitive measurement of target antigen. Immunoassays are capable of detection without any analyte enrichment, purification or pretreatment, which is generally needed by standard methods such as HPLC, mass spectrometry or gas chromatography. In this regard, photoelectrochemical (PEC) immunoassays have attracted substantial research scrutiny for its desirable combination of the inherent sensitivity of the PEC bioanalysis and the specific bioaffinity properties of the immunomolecules towards detection of biomolecules [21]–[24].

Further, evidences suggest that various nanostructured FET based biosensors have shown remarkable output for fast clinical diagnosis applications [25]. For instance, multiple silicon nanowire (SiNW) FETs connected in parallel has

Manuscript received March 31, 2021; revised June 27, 2021 and August 19, 2021; accepted September 10, 2021. Date of publication September 13, 2021; date of current version December 31, 2021. *(K. Sinha and B. Chakraborty contributed equally to the work.) (Corresponding author: C. Das Mukhopadhyay.)*

K. Sinha, S. Som Chaudhury, and C. Das Mukhopadhyay are with the Centre for Healthcare Science and Technology, IIEST, Howrah 711103, India (e-mail: ksinha2110@gmail.com; somchaudhurysutapa@gmail.com; chitrangadam@chest.iiests.ac.in).

B. Chakraborty and C. Roy Chaudhuri are with the Department of Electronics and Telecommunication Engineering, IIEST, Howrah 711103, India (e-mail: rnk4928@gmail.com; chirosreepram@gmail.com).

S. K. Chattopadhyay is with the Department of Chemistry, IIEST, Howrah 711103, India (e-mail: shyamalchattopadhyay@gmail.com).

Digital Object Identifier 10.1109/TNB.2021.3112534

been reported to successfully detect dopamine (DA) down to 10 picomolar (pM) with superior specificity in presence of other structurally similar chemical analogues [26]. A recent study with SiNW-FET immunosensor has been evidenced for detection of γ-amino butyric acid (GABA) with a detection limit as low as 970 femtomolar (fM) [27]. In addition, nanomaterials such as carbon nanotubes (CNTFETs) have also been implemented for detection of DA non-enzymatically with high sensitivity and selectivity enabling detection limit down to fM range [28]. Most of the reported works are mainly focused on SiNW and CNTs, only few studies have been evidenced to be focused on the detection of neurotransmitters using oxide semiconductor. However, the unstable SiNW surfaces can be easily oxidized and form an insulating layer which may degrade the device reliability and sensitivity, while the chirality of CNTs remains an unsolved problem. Thus, it's worthwhile to investigate metal oxide material for biosensing application [29].

Zinc oxide (ZnO) based thin film transistors have some attributes like minimized noise levels with large on-off ratio and are regarded as emerging high performance sensor platforms [30], [31]. High isoelectric point (9.0) and adequate electron transfer features have made ZnO a significant matrix for biosensing applications. Compared to other matrices, biocompatibility of ZnO hinders denaturation and conserves the critical structure of the captured protein [32]. Motivated to push down the limit of detection and overcome the disadvantages of prolonged response time with low binding kinetics of 2D nanostructure, 3D biosensors using ZnO has been developed by growing vertically directed ZnO nanorods for virus, proteins, macromolecules and enzyme diagnosis [33]–[44]. Single crystalline ZnO nanorods are structurally uniform with minimal dislocations and the spacing can be reduced to size scales that are commensurate with the size of the biomolecular analytes. FETs with nanorods are found to be impressive, robust and economically feasible platforms to achieve high current amplification and sustain an enhanced signal-to-noise ratio among all the detection methodologies owing to their excellent sensitivity, label-free, real-time response for biomolecule detection [45]. Moreover, ZnO nanorods based biosensors have paved their path into wearable since they can be fabricated on flexible substrates [46], [47].

Recently, a novel NaYF4:Yb,Tm@ZnO-based photoelectrochemical biosensor has been evidenced for determination of carcino-embryonic antigen (CEA). In this experiment ZnO has been uniformly covered on the surface of NaYF4: Yb, Tm by the process of calcination so that ZnO can be excited in situ by ultraviolet light from NaYF4: Yb, Tm to generate photocurrent, extending the application of metal-organic frameworks (MOF) derived photoelectric materials. The biosensor showed excellent selectivity and sensitivity with a detection limit of 0.032 ng mL-^{1} [48]. However, this detection limit may not be satisfactory for all types of biomolecules. In view of performance enhancement, ZnO nanorod FET-based biosensor has been fabricated for phosphate detection [36]. Recently, ZnO nanorods based FET biosensor has been reported towards rapid sensing of 5-HT with 1fM detection limit [49]. As ZnO is polycrystalline, it has got several defect states. These defect states regulate some effective FET parameters such as: on-off ratio, threshold voltage, field-effect mobility and transconductance. Therefore, it is significant to examine the effect of the above-mentioned defects on the detection limit as well as the sensitivity of FET biosensors. Besides, roughness of the surface also changes due to the presence of surface defects, which is expected to determine receptor binding density, longevity and selectivity of these sensors. Thus, optimization of the effect of defect state density in ZnO FET based biosensor is an essential criterion to enhance the performance. Surface roughness and defect state density related to ZnO FET have been optimized in a previous work [50]. Though ZnO based FET sensors have attracted considerable attention, their response is significantly non-linear and there has been no appreciable endeavor for improving the non-linearity, which is also beneficial for translation of such devices to point-of-care applications.

In this communication, we have introduced embedded gate electrode encompassing the channel of the FET which improves the uniformity in electric field line distribution through the electrolyte and proportionately enhances the capture of target biomolecule at ultra-low concentrations, thereby increasing the linearity. Further, we have incorporated the optimized parameters of ZnO nanorods reported previously, for rapid and selective detection of 5-HT. Key to our biosensor is its capability of selective, sensitive and linear detection down to 0.1fM in buffer as well as in real samples by electrical change on the basis of immunoreactions.

II. Materials/Experimental

A. Chemicals

Monoclonal antibody against 5-HT (MAB 352), clone YC5/45 has been purchased from Merck, EMD Millipore. Serotonin hydrochloride (C_{10} $H_{12}N_2O.HCl$), ascorbic acid (AA) ($C_6H_8O_6$) and dopamine hydrochloride ($C_8H_{11}NO_2.HCl$) have been procured from Sigma-Aldrich, USA. Distilled and de-ionized water (DI) has been obtained from the Milli-Q system (18.52 MΩ cm). Ethyl alcohol (C_2H_5OH), 3-mercaptopropyltrimethoxysilane (MTS), N-γ-maleimidobutyryloxysuccinimide (GMBS), sulphuric acid (H_2SO_4) and all other chemicals have been procured from Sigma-Aldrich, USA. Therefore, these chemicals have been utilized without further purification.

B. Synthesis of ZnO Nanorod-Based FET

Embedded gate electrode and interdigited source, drain electrodes have been fabricated on top of glass substrate using photolithography. The detailed lithography procedure has been indicated in earlier report [45]. This is followed by deposition of a layer of Cr (20 nm)/Au (100 nm) by thermal evaporation and the electrode patterns have been defined by lift-off process. In the next step, the poly methyl methacrylate (PMMA) solution has been spin coated on the substrates at 3000 rpm for 30 s. After baking at 180 °C for 30 mins, a 1.3 μm thick PMMA layer has been obtained. The predesigned patterns with opening on the ZnO regions have been transferred on the PMMA photoresist layer by the mask aligner.

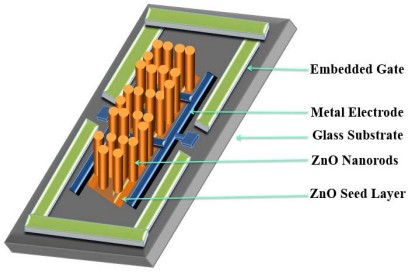

Fig. 1. The schematic of the sensor.

The substrate with exposed PMMA layer has been dipped into a developing solution (methylisobutylketone and isopropanol at volume ratio of 1:3) to produce the patterned features. After developing for 60 s, the substrate has been dipped into isopropanol for 60 s to wash off the developing solution and then dried under nitrogen flow. In the next step, ZnO seed layer has been synthesized incorporating E-beam deposition method. Time of deposition has been set to 120 sec. The detailed synthesis method has been reported in previous work [50]. ZnO nanorods have been synthesized on top of the ZnO seed layer using hydrothermal technique as indicated in earlier report [45]. The ZnO nanorods were mainly synthesized using equimolar zinc nitrate hexahydrate [$Zn(NO_3)_2$,$6H_2O$] and hexamethylenetetramine (HMTA:$C_6H_{12}N_4$). 50mM zinc nitrate hexahydrate was mixed with 100 ml of DI water in order to prepare the ZnO precursor solution. Following this, the solution bath was heated by keeping on a magnetic stirrer. Finally, the bath temperature reaches to 60 °C then 4 ml of ammonium hydroxide [NH4OH] was added to the solution. Next, the entire solution was kept on stirring for another 30mins and was kept undisturbed for another 24 hours. Again equimolar concentration of zinc nitrate hexahydrate and hexamethylenetetramine was mixed respectively with 50ml of DI water and stirred for 10mins. After this both the bath solutions have been mixed together and gradually stirred at 260rpm. Finally, for better crystallization the ZnO nanorods were properly annealed at 350 °C for approximately 5mins by using rapid thermal annealing method. The whole hydrothermal method has been represented chemically by Eqs. (i-iv):

$$C_6H_{12}N_4 + 6H_2O \rightarrow 6HCHO + 4NH_3 \quad \text{(i)}$$
$$NH_3 + H_2O \rightarrow NH_4^+ + OH^- \quad \text{(ii)}$$
$$2OH^- + Zn^{2+} \leftrightarrow Zn(OH)_2 \quad \text{(iii)}$$
$$Zn(OH)_2 \leftrightarrow ZnO + H_2O \quad \text{(iv)}$$

Next, the substrate has been immersed in acetone for 30 mins to dissolve the PMMA templates. The sample has been then removed from acetone and dried in air. The schematic of the sensor is depicted in Fig.1.

C. Functionalization of ZnO Surface

Fabricated ZnO nanorods have been treated with oxygen plasma to overcome various fluctuations occurring during the positioning of solution droplets and hence ensure the repeatability of measurements. After plasma treatment, the silanization process has been executed, followed by crosslinker

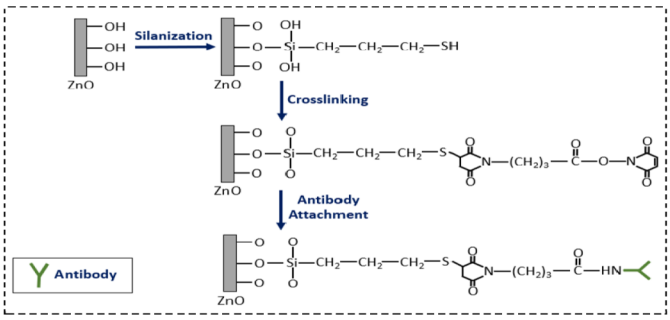

Scheme 1. The functionalization and antibody immobilization mechanism of the sensing surface.

attachment. In the next step, the sensors have been incubated with the optimized concentration of monoclonal antibody against 5-HT (1:1000) dilution to allow maximum binding of the antibody. Then, the non-specific adsorption of antibody has been removed by washing in 20mM phosphate buffer saline (PBS) (pH 7.2).This has been followed by blocking the sensor surface using 10μl bovine serum albumin(1mg/ml). The steps have been schematically represented in Scheme 1 and the detailed procedure has been outlined in previous report [45].

D. Serotonin Solution Preparation

Serotonin hydrochloride (1mg/ml) with ≥98% purified has been used as the target molecule to carry out the electrical measurements. Serial dilutions have been performed using 100mM PBS (pH 7.2) to produce concentration ranging from 0.1fM-1nM. Moreover, spiking of serotonin hydrochloride in human blood serum has been done to carry out further measurements in the physiological sample.

E. Preparation of Human Serum Samples

5ml each of 5 human blood samples have been collected from healthy volunteers with proper consent. The blood has been secured in sterilized plastic containers and further centrifuged at 3,000 rpm for 10 min, not later than 30 min after blood sampling. The obtained serum has then been kept in sterilized plastic containers and has been equilibrated with PBS (pH 7.2) for further utilization in electrical studies.

F. Electrical Measurement of Serotonin

A sensor holder set up has been used to interface each sensor chip with the PC. In the experimental setup, sensors' bond pads have been set just beneath the sensor holder probes. Then, the sensor holder probes have been connected with the drain, as well as source electrodes, and are mainly spring-loaded along with the adjustment screws which align them with the bond pads. The liquid gate electrode has been fitted by means of a small gap in the experimental setup and has been soldered to a metallic interconnect. Furthermore, the gate electrode has been fixed to a dc power supply (Keysight technologies). A high-frequency signal of 20 mV amplitude has been applied at the drain electrode through a signal generator (Agilent33521 A) with the frequency ranging from 200-1000 kHz. A lock-in amplifier

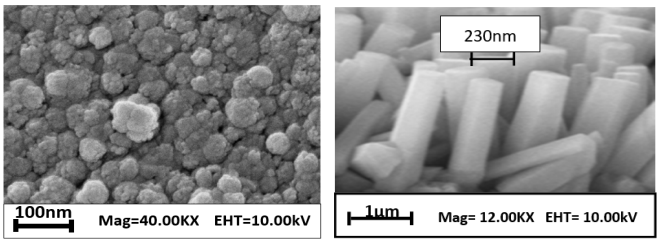

Fig. 2. (a) FESEM image of ZnO seed layer, (b) FESEM image of ZnO nanorod.

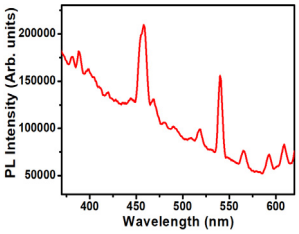

Fig. 3. PL spectrum for ZnO nanorod at room temperature.

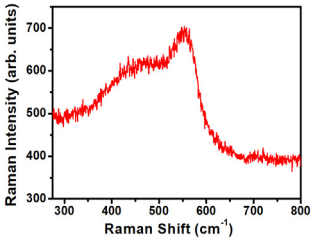

Fig. 4. Raman spectrum of ZnO.

(Stanford Research, SR 830) has been used for modulation of high- frequency signal with a reference signal of 1.43 kHz and has been provided to the ZnO nanorod FET at the source terminal. When the root mean square value of the mixing current stabilizes after application of 100 μl buffer, 10 μl of analyte has been pipetted. For both before and after analyte applications, the root mean square value of the mixing current has been recorded at the modulated frequency through the drain terminal. The steady-state analysis has been performed with spiked 5-HT solutions, both in buffer and serum samples. For real-time analysis, measurements have been recorded with a computer interface using a control solution at a sampling rate of 0.075 kHz.

A set of five parallel replicates has been recorded for each sample. The mean values along with the standard deviations have been plotted. Limit of detection (LOD) has been estimated as that 5-HT concentration for which the mixing current is at least 3 times the standard deviation from the mean baseline value. The accuracy of the detection method has been calculated as the percentage of recovery by adding 0.1 fM, 1 pM and 1 nM solution of 5HT to aliquots of a blank serum sample. Percent of recovery is the ratio of the amount of antigen solution which actually gets collected to the amount of antigen solution which is supposed to collect.

G. Implementation of Characterization Techniques

The morphological characterization of the surface has been conducted by the field-emission scanning electron microscopy (ZEISS EVO-MA 10).The crystal structure and unit cell dimensions of ZnO has been carried out by X-Ray diffraction (XRD) (Rigaku SmartLab X-ray diffractometer). On the other hand, Raman spectroscopy and photoluminiscence spectrometry (PL) measurements of the ZnO nanorods have been carried out using Raman and MicroPL System (HORIBA-LabRAM HR Evolution).

III. Results and Discussion

A. Characterization Results of Optimized Sensor

The surface morphology has been evidenced by high-resolution FESEM setup. Fig. 2a depicts the formation of ZnO seed layer and Fig.2b shows the profusely dense and vertically arranged ZnO nanorods with the length to be approximately 1.54μm along with the diameter of around 230 nm. PL has been done at room temperature and Fig. 3 depicts the PL spectrum for ZnO nanorod grown on glass substrate. Two main peaks can be observed from the spectrum: first, near band edge emission (NBE) and second, deep level emission (DLE). NBE peak gets generated due to the excitonic recombination around bandgap of ZnO in the ultra violet (UV) region. DLE peak corresponds to the existence of several defects such as oxygen antisite (O_{Zn}), oxygen vacancy (V_O) and zinc vacancy (V_{Zn}). From Fig. 3 it can be seen that NBE of ZnO nanorods occur at 389 nm and distinct DLE peaks are at blue (458 nm), green (519 nm, 541 nm and 565 nm) and orange (592 nm and 609 nm) range. Presence of defects in ZnO gives rise to various defect energy states in between the bandgap of ZnO which can tune ZnO based FET devices' performance. It may be observed from the PL measurements that the NBE/DLE ratio of the optimized sensor is 1.206.

The Raman spectra of the grown ZnO FET fabricated on glass substrates represented at Fig. 4. In the spectra, several Raman modes have been identified near 441 cm^{-1} and 571 cm^{-1}. The E2 (high) mode of ZnO was represented by the band at 441 cm^{-1}whereas, the A1 longitudinal optical (LO) mode was represented at 571 cm^{-1}. The E2 (high) mode corresponds to the characteristic of wurtzite lattice. The A1 (LO) mode generates from the defects of V_O.

The crystallinities of ZnO nanorods have been examined by XRD patterns. It is evident from the XRD spectrum that (002) is the preferred direction of hexagonal wurtzite crystalline ZnO nanorods. ZnO nanorods have a tendency to grow with a preferable c-axis orientation due to (002) plane's lowest surface free energy. A competitive growth occurs between the adjacent crystallites, until the rapid generation crystallite overcomes the ones with sluggish growth and proceeds to the free surface. (002) peak intensity at $2\theta = 34.24°$ is quite sharp as can be confirmed from the Fig. 5.

B. Finite Element Simulation

For estimating the biomolecule capture using the embedded electrode, electric potential distribution in the electrolyte has been simulated using finite element method of COMSOL Multiphysics 4.3b. AC/DC module has been selected to

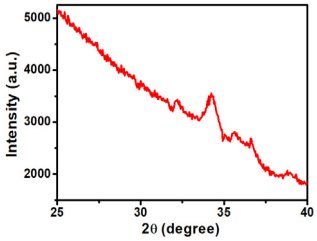

Fig. 5. XRD spectrum of ZnO nanorods.

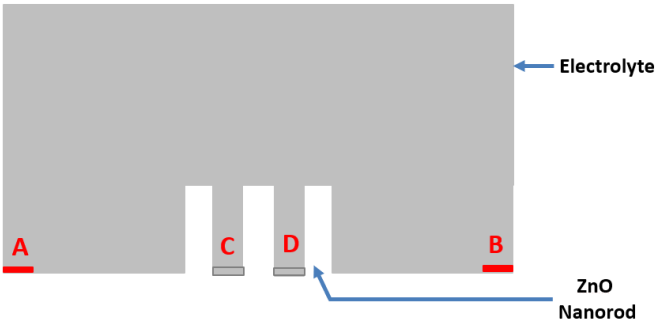

Fig. 6. Schematic of case 1 (Not drawn to scale).

incorporate required physics. Two cases have been studied here. In case 1, positive potential has been applied at the two embedded electrode terminals (A and B) and the bottom electrodes (C and D), corresponding to source and drain have been kept grounded. All other boundaries have been indicated as insulation. The distance between the embedded electrodes and the active regions is 500 μm and the height of the electrolyte is 1 mm. The sensor geometry has been simplified showing a few nanorods of length 1.5 μm and diameter 230 nm(in accordance with the FESEM results), to reduce the computational complexity. The schematic representation of the structure simulated is shown in Fig.6. A high-density mesh has been considered within the constraint of executing the simulation in reasonable time. Computational domain has assumed room temperature with the parameters, $\varepsilon_r = 81$, $\eta = 2 \times 10^{-5}$Pa.s, $\sigma = 1.6$ S/m where ε_r is the relative permittivity, η is the dynamic viscosity and σ is the conductivity of the electrolyte. In the steady state continuum regime, the electric field distribution is guided by Maxwell-Boltzman theory (Eq. (1)) which describes the potential distribution within nanorods:

$$\nabla \cdot (\varepsilon \nabla V) = -q(p - n - C) \tag{1}$$

where $C = N_D - N_A + \rho_p - \rho_n$, q is the electron charge, ε is the permittivity, p and n are the hole and electron concentrations respectively and C is the concentration of additional, typically fixed, charges. These fixed charges can originate from charged impurities of donor (N_D) and acceptor (N_A) and from trapped holes (ρ_p) and electrons (ρ_n).

To solve the model, current continuity equations (Eq. (2)) have been used:

$$\frac{1}{q}\nabla \cdot J_n = -U_n; \quad \frac{1}{q}\nabla \cdot J_p = -U_p \tag{2}$$

where $U_n = \sum R_{n,i} - \sum G_{n,i}$ is the net electron recombination rate from all generation ($G_{n,i}$) and recombination mechanisms ($R_{n,i}$). Similarly U_p is the net hole recombination rate from all generation ($G_{p,i}$) and recombination mechanisms ($R_{p,i}$).

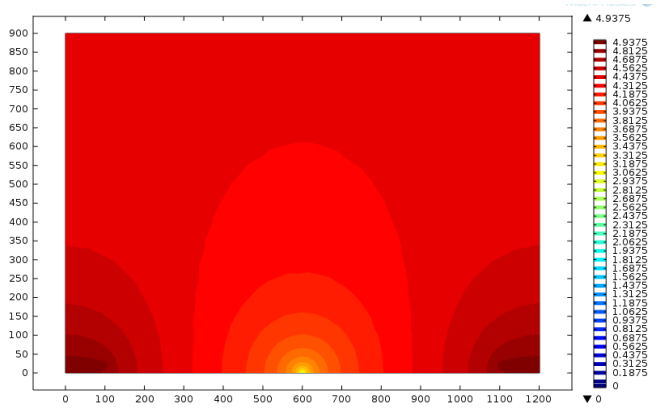

Fig. 7. Potential distribution of case 1.

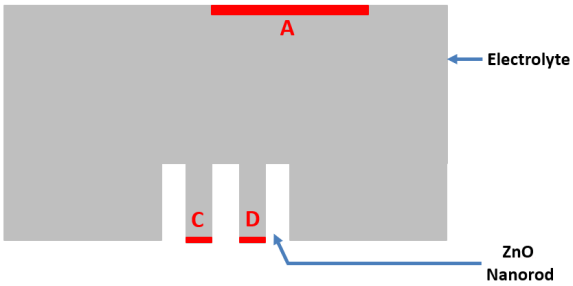

Fig. 8. Schematic of case 2 (Not drawn to scale).

Potential distribution plot related to case 1 has been depicted in Fig. 7. The nanorods are not prominently visible since their dimensions are much smaller than the electrodes and the spacings. This situation corresponds to uniform field line distribution within the electrolyte which is expected to result in electrophoretically driven proportional biomolecule capture over the entire range, unless steric hindrance effects appear for very high concentration. Case 2 represents the suspended gate electrode which is conventionally deployed in FET biosensor. In majority of the cases, the gate electrodes are significantly larger in dimension than the FET channel and hence may be positioned anywhere in the electrolyte volume. Thus, the probability of asymmetric placement with respect to the active sensor region is considerable. Positive potential has been provided at terminal A which refers to the liquid gate electrode. The bottom electrodes (C and D) have been kept grounded. Schematic has been shown in Fig. 8. It is observed from the potential distribution plot in Fig.9 that, uniform distribution of electric potential cannot be seen as the electrolyte solution amount is different in both sides of the liquid electrode terminal. This is expected to result in disproportionate capture of biomolecules in the low concentration regime due to their non-uniform distribution, which in turn is responsible for the non-linearity. This highlights the importance of a uniformly encompassing embedded gate electrode in ZnO FET biosensors.

C. FET Measurements and Limit of Detection (LOD)

The measurement of 5-HT is of importance because it can provide supporting information to understand the role of

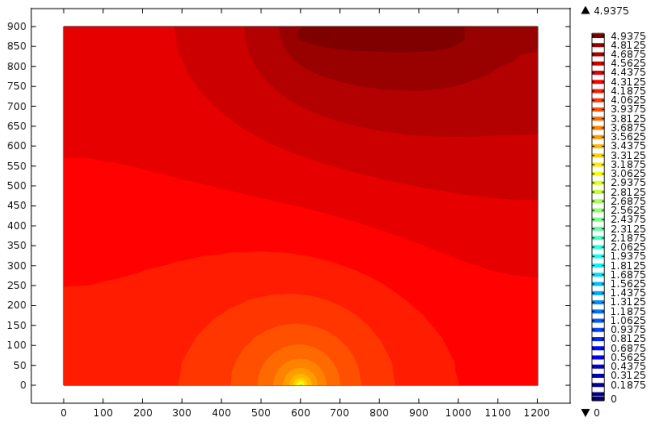

Fig. 9. Potential distribution of case 2.

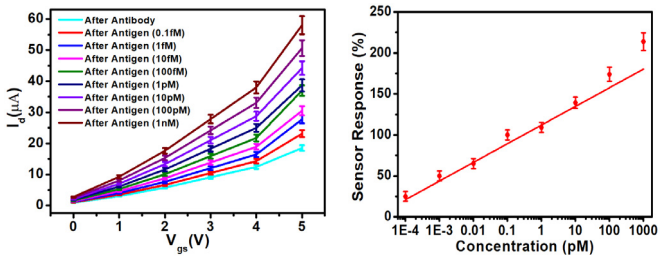

Fig. 10. (a) Curve showing variations in drain current (I_d) with gate to source voltage (V_{gs}) after antibody immobilization and after capture of different 5-HT concentrations in presence of 100 mM buffer (pH 7.2) and (b) variation of sensor response with different 5-HT concentrations in 100 mM buffer.

5-HT in neurological disordered syndromes, thereby improving clinical treatment efficiency. For this purpose, the FET response of the ZnO nanorods has been applied to detect 5-HT in real samples and 100 mM PBS solution (pH 7.2). The fabricated ZnO nanorods are of 230 nm diameter and length of 1.54 μm approximately. In Fig. 10(a), the curve of drain current variations (I_d) with gate to source voltage (V_{gs}), after antibody immobilization and after capture of various concentrations of antigen (5-HT) registered in 100 mM buffer (pH 7.2) has been recorded at 1MHz frequency keeping drain to source voltage (V_{ds}) fixed at 5V. The selection of frequency has been optimized earlier for ZnO nanorods [45]. The data represented is the mean value of I_d along with the standard deviations recorded for every antigen concentration, after testing with five sensors. In this whole experiment, every sensor has been exposed to only one concentration of antigen and after that the sensor has been discarded since for practical applications, each sensor is used once to ensure reliability. Thus, every sensor has undergone random exposure and not any systematic increase or decrease in antigen concentration.

It has been observed that I_d increases by one order of magnitude in case of a typical change of V_{gs} from 0 to 5 V, thereby indicating high transconductance. This may be attributed to the fact that the surfaces of the n-type ZnO nanorods are usually depleted due to the chemisorptions of oxygen molecules while the core which is electrically neutral, is conducting. As gate voltage increases, the width of the depletion region decreases significantly which leads to a noticeable increase in conductance. The relationship between

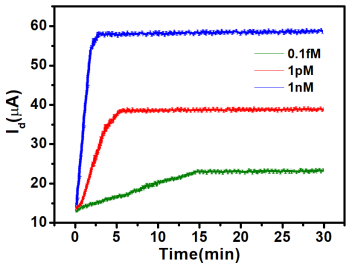

Fig. 11. Real-time response of the ZnO nanorod FET based biosensor in three different 5-HT concentrations spiked in controlled solutions.

I_d and V_{gs} can be expressed by Eq. 3 which has also been reported by other researchers [51].

$$I_d = \left(V_{gs}^2 + C_1 V_{gs} + C_2\right) C_3 \tag{3}$$

where, C_1, C_2 and C_3 are fitting constants.

It can be evidenced that with increasing concentration of 5-HT within the wide dynamic range of 0.1fM to 1nM, there is a remarkable increase in I_d of the transistor. As the 5-HT molecules are positively charged, carrier accumulation takes place on the ZnO nanorods surface, since ZnO is intrinsically n-type. Thus, the electron accumulation within nanorods results in increase of I_d and a decrease in net resistance after antigen capture. As the current characteristics along with its standard deviation for 0.1 fM concentrations of 5-HT shifts by more than 3 times from the standard deviation of I_d curve after antibody immobilization, the LOD achieved is 0.1 fM in buffer. Sensor response was evaluated as the fractional change in I_d corresponding to V_{gs} of 5V, for a particular concentration of 5-HT and this has been expressed as percentage in Fig. 10(b). It has been observed that the relative standard deviations (RSD) obtained from the replicates are within 5%. From Fig. 10(b) it is also evident that the nature of sensor response depicts linearity with antigen concentration in buffer.

Fig. 11 shows the real-time response of the ZnO nanorod FET based biosensor in three different 5-HT concentrations spiked in controlled solutions. The change in I_d has been recorded with time to study the stability of current after 5-HT capture. It has been observed from the normalized I_d characteristics that the time taken to achieve steady-state is around 15 min for 0.1 fM and only 2 min for 1 nM concentration. This may be attributed to the fact that lower the concentration of the analyte, slower is the rate of diffusion towards the sensor surface [52]. Hence, a detection time of approximately 20 min for a trace concentration of 0.1 fM is remarkably better than that of the conventional methods which requires around 3hr for detection of 26 nM concentration of 5-HT [53]. Further the standard deviations obtained from the replicates are within 6% for all the concentrations.

D. Interference Studies

5-HT is found only in minimal amount in the human body. Hence, the presence of similarly structured molecules or physiological compounds or various medicinal drugs might influence the accuracy of existing detection methods for this analyte. In the present study, the selectivity of the ZnO FET for

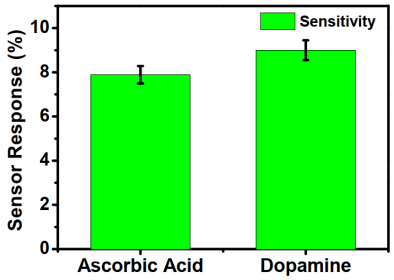

Fig. 12. Specificity of the ZnO nanorod FET based biosensor towards 5-HT detection.

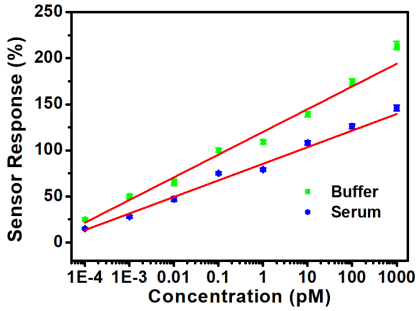

Fig. 13. Variation of sensor response with different 5-HT concentrations in buffer and serum for 1MHz frequency.

5-HT detection has been examined by means of competitive binding tests with similar catecholamine structure such as DA and other biological molecules like AA with redox potential close to that of 5-HT. Moreover, these compounds exist simultaneously in physiological fluid and due to their identical structure, might hamper the binding of 5-HT to the antibody sites. The specificity experiments was executed by monitoring the sensor response, keeping V_{gs} constant at 5V using AA and DA molecules at 1nM buffer. Therefore, the resulted observation from Fig. 12 depicted that the sensor response was found to be within 9% for such high concentration, which indicates appreciable specificity of the ZnO biosensor.

E. Real-Sample Analysis

A huge number of pathophysiological conditions have been attributed to the various levels of 5-HT in blood [54]. Therefore, to investigate the suitability of the proposed biosensor in complex biomatrix, serum samples have been used for analysis using the potent spike method under optimized conditions [55]. In this study, different 5-HT concentrations have been spiked in serum and tested with the same sensor. The non-specific molecules present in the serum which are outside the Debye length do not modulate the gate voltage significantly and hence the FET response is not affected, leading to real time detection even for complex samples [27]. It has been deciphered that the sensor response decreases for real sample in comparison to buffer solution, and this phenomenon can be justified by the fact that lower number of target molecules gets captured for the equal quantity of pipetted solution. Detection limit has been considered to be that concentration of 5-HT for which the deviation of the sensor response is less than 1/5th of the mean value of the signal. Here detection limit is 0.1 fM. From the sensor response, the concentration of 5-HT has been estimated with the help of the characteristics shown in Fig. 13.

The sensor response depicted in Fig. 13 is the calibration curve. Sensor response has been calculated as the fractional change in current before and after antigen capture as given in equation 4:

$$S = \frac{\partial I_d}{I_d} \tag{4}$$

where, S is the sensor response. It is observed that the sensor response in serum is appreciably linear with logarithm of 5-HT concentration in the range of 0.1 fM to 1 nM. The mean characteristics have been fitted by a linear function as depicted by equation. 5:

$$y = a + blog(x) \pm \delta_1 \pm \delta_2 \tag{5}$$

where, a and b are fitting parameters along with respective standard deviations of δ_1 and δ_2, y is the sensor response and x is the concentration of 5-HT.

TABLE I
RECOVERY STUDY OF THE BIOSENSOR

5-HT added	5-HT found	Recovery (%)
0.1 fM	0.3 fM	300
1 pM	1.2 pM	120
1 nM	0.8 nM	80

In order to assess recovery of the developed biosensor, the sensor has been exposed to three different concentrations of spiked serum samples, as indicated in Section IIF. For unknown samples, experimental data provides the values of y obtained from five sensors. For different values of y, x have been extracted from equation 5 and the corresponding mean along with standard deviations have been estimated. This mean value is the 5-HT concentration actually recovered from the sample. Satisfactory recovery has been achieved, as shown in Table I. The sensor performance has also been validated by means of conventional immunoreactions enzyme-linked immunosorbent assay (ELISA) (ImmuSmol ELISA Kit). For this purpose, seven test solutions of 5-HT in real sample such as blood serum was prepared and the obtained results from both the methods are indicated in Table II. As the detection limit of the proposed sensor is lower than the ELISA kit, higher concentrations of 5-HT solutions have been prepared for testing with the latter which then was diluted by a known factor, before undergoing experimentation with the sensor. Next, the measurements obtained from the commercial system was further divided by the known dilution factor and thereby, correlated with that from the sensor. Though the sensor equation and the ELISA reader generate output up to three places of decimal, it does not have much practical significance since the actual concentration of the molecule in the solution which has been prepared by serial dilution cannot be measured with such precision. Thus the data has been represented with one place of decimal. Each unknown sample has been tested with ten different sensors. Table II shows that both the mean results and the standard deviations obtained from our sensor and the ELISA method is close. However, the accuracy of the biosensor is slightly degraded from that of

TABLE II
COMPARISON OF THE RESULTS OBTAINED FROM ZNO NANOROD FET BASED BIOSENSOR WITH ELISA METHOD

Sample No.	Test Solutions	Measured by sensor	Measured by ELISA
1.	0.5 fM	0.5fM ± 0.02fM	0.5fM ± 0.01 fM
2.	2 fM	2.6 fM ± 0.05fM	2.5 fM ± 0.04fM
3.	20fM	20.5 fM ± 0.1 fM	20.4 fM ± 0.4fM
4.	500 pM	502 pM ± 9.1pM	502 pM ± 9pM
5.	300pM	303 pM ± 6.1pM	302.1pM ± 6 pM
6.	20pM	22 pM ± 0.4pM	21 pM ± 0.4pM
7.	500 fM	502 fM ± 10.1fM	501 fM ± 10.2fM

TABLE III
COMPARISON OF THE FABRICATED BIOSENSOR WITH EXISTING BIOSENSORS

Ref.	Method of detection	Neuro-transmitters	LOD	Selectivity	Rapid Detection	Linear Range
[57]	Gold nanorattles decorated reduced	5-HT	0.387 pM	Citric acid, uric acid, glutamic acid,		3×10^{-6} M to $1x10^{-3}$ M
	graphene oxide electrochemical sensor			glucose, serum albumin, urea and alanine		
[23]	SiNW FET immunosensor	GABA	970fM		17 mins	970 fM to 9.7 µM
[58]	Electrochemical rotating droplet system	5-HT, DA	10nM (5-HT) 100nM (DA)			100 nM to 2 µM
[22]	SiNW FET sensor	DA	10pM		7 mins	10^{-11} to 10^{-8} M
[59]	Tyrosinase based amperometric sensor	5-HT	0.84M		20 mins	4 to 140 - µM
[24]	Non-enzymatic CNTFET sensor	DA	1fM		5 mins	1pM to 0.1µM
This paper	Optimized ZnO nanorod FET immunosensor	5-HT	0.1fM	Ascorbic acid	20 mins	0.1fM to 1nM

the ELISA. This does not have significant clinical impact [56]. Hence, the proposed label free sensor has potential for point-of-care applications, even if the accuracy is marginally low in comparison to labelled ELISA techniques. For the sensor to be commercialized, a dedicated signal processing unit needs to be interfaced along with appropriate packaging. Most importantly, extensive clinical trials have to be performed by collecting patients' samples from hospitals, after which the proposed system may receive formal approval for practical deployment.

The performance of the biosensor has been compared with existing reports as shown in Table III. Selectivity issue has not been addressed by most of the reported articles whereas this work demonstrates selectivity of the biosensor with ascorbic acid. It has been found that the fabricated ZnO FET biosensor lowers the detection limit to 0.1fM which is at least one order of magnitude lower than the existing reports. Compared to other reports, our FET biosensor has got wide linear range from 0.1 fM to 1 nM and detection time is about 20 mins.

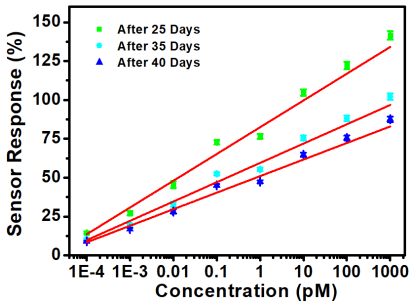

Fig. 14. Variation of sensor response with different 5-HT concentrations in serum after 30 days, 40 days and 60 days.

F. Reproducibility and Stability Studies of the ZnO Nanorod FET-Based Biosensor

Reproducibility, as well as stability, are crucial analytical parameters in terms of commercialization of the sensor [60], [61]. In order to examine the reproducibility of the fabricated ZnO nanorod FET based biosensor, current responses have been simultaneously recorded for five separate batches of sensors. The result depicted that both the baseline current and the modified current after analyte exposure changes within 4% from one batch to another, thereby proving that the fabricated sensor is significantly reproducible. In order to study the stability of the fabricated ZnO nanorod FET based biosensor, the sensor response has been taken into consideration for 60 days after immobilization of antibody and refrigerating at −20°C. There has been a negligible change in baseline I_d and 90% of the original current signal has been observed to be preserved after 40 days, which has been evaluated at a regular interval of 10 days, while I_d gradually decreases to 60% after 60 days, proving that the sensor is stable for maximum 60 days. Fig.14 displays sensor response with various antigen concentrations after different storage times. A 3%, 30% and 40% reduction in original sensor response values have occurred after 30 days, 40 days and 60 days respectively. The decay may be attributed to the denaturation of the antibody molecules.

IV. CONCLUSION

In this study, it has been summarized that ZnO nanorod FET based biosensor with embedded gate electrode encompassing the FET channel improves the uniformity of the electrical field line distribution through the electrolyte and thereby, increases the capture of the targeted biomolecule at very low concentrations, resulting in enhanced linearity. Additionally, the optimized defect states and surface roughness along with immobilized antibody enable label-free detection of 5-HT with detection limit as low as 0.1fM in buffer as well as in real serum. Several concentrations of 5-HT ranging from 0.1fM to 1nM have been efficiently measured by the sensor and validated with commercially available assay kits. Moreover, the detection time for 0.1 fM is approximately 20 mins, which is much better than the existing methods. The fabricated biosensor also possesses excellent selectivity, reproducibility and stability. In addition, this ZnO nanorod FET based system can be anticipated towards a potent miniaturized biosensing device for accurate diagnosis of various central nervous system

disorders and also can be further exploited for providing a low-cost platform for the development of implantable biochip for detection of 5-HT as disease biomarker within the brain.

REFERENCES

[1] D. G. Grahame-Smith, "The carcinoid syndrome," *Amer. J. Cardiol.*, vol. 21, no. 3, pp. 376–387, 1968.

[2] M. Camilleri and D. A. Katzka, "Irritable bowel syndrome: Methods, mechanisms, and pathophysiology. Genetic epidemiology and pharmacogenetics in irritable bowel syndrome," *Amer. J. Physiol., Gastrointestinal Liver Physiol.*, vol. 302, no. 10, pp. 1075–1084, 2012.

[3] B. J. Jones and T. P. Blackburn, "The medical benefit of 5-HT research," *Pharmacol. Biochem. Behav.*, vol. 71, no. 4, pp. 555–568, Apr. 2002.

[4] S.-H. Lin, L.-T. Lee, and Y. K. Yang, "Serotonin and mental disorders: A concise review on molecular neuroimaging evidence," *Clin. Psychopharmacol. Neurosci.*, vol. 12, no. 3, pp. 196–202, Dec. 2014.

[5] C. Maximino, *Serotonin in the Nervous System of Vertebrates*. New York, NY, USA: Springer, 2012.

[6] K. Hara, Y. Hirowatari, Y. Shimura, and H. Takahashi, "Serotonin levels in platelet-poor plasma and whole blood in people with type 2 diabetes with chronic kidney disease," *Diabetes Res. Clin. Pract.*, vol. 94, no. 2, pp. 167–171, Nov. 2011.

[7] S. W. Watts, S. F. Morrison, R. P. Davis, and S. M. Barman, "Serotonin and blood pressure regulation," *Pharmacol. Rev.*, vol. 64, no. 2, pp. 359–388, Apr. 2012.

[8] G. M. Anderson, "Signal-to-noise optimization of HPLC-fluorometric systems and their application to the analysis of indoles," *Adv. Exp. Med. Biol.*, vol. 294, pp. 51–61, 1991.

[9] M. Sa, L. Ying, A.-G. Tang, L.-D. Xiao, and Y.-P. Ren, "Simultaneous determination of tyrosine, tryptophan and 5-hydroxytryptamine in serum of MDD patients by high performance liquid chromatography with fluorescence detection," *Clin. Chim. Acta*, vol. 413, nos. 11–12, pp. 973–977, Jun. 2012.

[10] J. Dorszewska, J. Florczak-Wyspianska, M. Kowalska, M. Stanski, A. Kowalewska, and W. Kozubski, *Serotonin in Neurological Diseases*. Rijeka, Croatia: InTech, 2017.

[11] C. D. Mukhopadhyay, B. Ruidas, and S. S. Chaudhury, "Role of curcumin in treatment of Alzheimer disease," *Int. J. Neurorehabil.*, vol. 4, no. 3, 2017, Art. no. 1000274.

[12] S. Som Chaudhury *et al.*, "A novel PEGylated block copolymer in new age therapeutics for Alzheimer's disease," *Mol. Neurobiol.*, vol. 56, no. 9, pp. 6551–6565, Sep. 2019.

[13] E. C. Y. Chan, P. Y. Wee, P. Y. Ho, and P. C. Ho, "High-performance liquid chromatographic assay for catecholamines and metanephrines using fluorimetric detection with pre-column 9-fluorenylmethyloxycarbonyl chloride derivatization," *J. Chromatogr. B, Biomed. Sci. Appl.*, vol. 749, no. 2, pp. 179–189, Jan. 2000.

[14] M.-M. Hsieh and H.-T. Chang, "Discontinuous electrolyte systems for improved detection of biologically active amines and acids by capillary electrophoresis with laser-induced native fluorescence detection," *Electrophoresis*, vol. 26, no. 1, pp. 187–195, Jan. 2005.

[15] T. Yoshitake, J. Kehr, K. Todoroki, H. Nohta, and M. Yamaguchi, "Derivatization chemistries for determination of serotonin, norepinephrine and dopamine in brain microdialysis samples by liquid chromatography with fluorescence detection," *Biomed. Chromatogr.*, vol. 20, no. 3, pp. 267–281, 2006.

[16] Z. Peterson, M. Lee, and S. Graves, "Determination of serotonin and its precursors in human plasma by capillary electrophoresis–electrospray ionization–time-of-flight mass spectrometry," *J. Chromatogr. B, Anal. Technol. Biomed. Life Sci.*, vol. 810, no. 1, pp. 101–110, Oct. 2004.

[17] E. Maurer-Spurej, K. Dyker, W. A. Gahl, and D. V. Devine, "A novel immunocytochemical assay for the detection of serotonin in platelets," *Brit. J. Haematol.*, vol. 116, no. 3, pp. 604–611, Mar. 2002.

[18] S. Sharma, N. Singh, V. Tomar, and R. Chandra, "A review on electrochemical detection of serotonin based on surface modified electrodes," *Biosensors Bioelectron.*, vol. 107, pp. 76–93, Jun. 2018.

[19] T. Sakata, "Biologically coupled gate field-effect transistors meet *in vitro* diagnostics," *ACS Omega*, vol. 4, no. 7, pp. 11852–11862, Jul. 2019.

[20] S. K. Kim, D. Kim, and S. Jeon, "Electrochemical determination of serotonin on glassy carbon electrode modified with various graphene nanomaterials," *Sens. Actuators B, Chem.*, vol. 174, pp. 285–291, Nov. 2012.

[21] J. Shu and D. Tang, "Current advances in quantum-dots-based photoelectrochemical immunoassays," *Chem. Asian J.*, vol. 12, no. 21, pp. 2780–2789, Nov. 2017.

[22] L. Huang, J. Chen, Z. Yu, and D. Tang, "Self-powered temperature sensor with Seebeck effect transduction for photothermal–thermoelectric coupled immunoassay," *Anal. Chem.*, vol. 92, no. 3, pp. 2809–2814, 2020.

[23] Z. Luo, Q. Qi, L. Zhang, R. Zeng, L. Su, and D. Tang, "Branched polyethylenimine-modified upconversion nanohybrid-mediated photoelectrochemical immunoassay with synergistic effect of dual-purpose copper ions," *Anal. Chem.*, vol. 91, no. 6, pp. 4149–4156, Mar. 2019.

[24] Y. Lin, Q. Zhou, D. Tang, R. Niessner, and D. Knopp, "Signal-on photoelectrochemical immunoassay for aflatoxin B_1 based on enzymatic product-etching MnO_2 nanosheets for dissociation of carbon dots," *Anal. Chem.*, vol. 89, no. 10, pp. 5637–5645, May 2017.

[25] K.-I. Chena, B.-R. Li, and Y.-T. Chen, "Silicon nanowire field-effect transistor-based biosensors for biomedical diagnosis and cellular recording investigation," *Nano Today*, vol. 6, no. 2, pp. 131–154, 2011.

[26] B.-R. Li, Y.-J. Hsieh, Y.-X. Chen, Y.-T. Chung, C.-Y. Pan, and Y.-T. Chen, "An ultrasensitive nanowire-transistor biosensor for detecting dopamine release from living PC12 cells under hypoxic stimulation," *J. Amer. Chem. Soc.*, vol. 135, no. 43, pp. 16034–16037, 2013.

[27] J.-H. Lee, E.-J. Chae, S.-J. Park, and J.-W. Choi, "Label-free detection of γ-aminobutyric acid based on silicon nanowire biosensor," *Nano Converg.*, vol. 6, no. 1, pp. 1–6, Dec. 2019.

[28] S. Joshi, V. D. Bhatt, A. Märtl, M. Becherer, and P. Lugli, "Regenerative, highly-sensitive, non-enzymatic dopamine sensor and impact of different buffer systems in dopamine sensing," *Biosensors*, vol. 8, no. 1, pp. 1–10, 2018.

[29] Y. L. Bunimovich, Y. S. Shin, W.-S. Yeo, M. Amori, G. Kwong, and J. R. Heath, "Quantitative real-time measurements of DNA hybridization with alkylated nonoxidized silicon nanowires in electrolyte solution," *J. Amer. Chem. Soc.*, vol. 128, no. 50, pp. 16323–16331, 2006.

[30] M.-S. Ahn, R. Ahmad, K. S. Bhat, J.-Y. Yoo, T. Mahmoudi, and Y.-B. Hahn, "Fabrication of a solution-gated transistor based on valinomycin modified iron oxide nanoparticles decorated zinc oxide nanorods for potassium detection," *J. Colloid Interface Sci.*, vol. 518, pp. 277–283, May 2018.

[31] B. Chakraborty and C. RoyChaudhuri, "Performance enhancement of biomolecule detection in ZnO thin-film transistor by noise spectroscopy measurements," *IEEE Sensors J.*, vol. 19, no. 23, pp. 10977–10984, Dec. 2019.

[32] Y. Cao, E. Galoppini, P. I. Reyes, Z. Duan, and Y. Lu, "Morphology effects on the biofunctionalization of nanostructured ZnO," *Langmuir*, vol. 28, no. 21, pp. 7947–7951, May 2012.

[33] N. R. Shanmugam, S. Muthukumar, and S. Prasad, "A review on ZnO-based electrical biosensors for cardiac biomarker detection," *Future Sci. OA*, vol. 3, no. 4, Nov. 2017, Art. no. FSO196.

[34] N. R. Shanmugam, S. Muthukumar, and S. Prasad, "Ultrasensitive and low-volume point-of-care diagnostics on flexible strips—A study with cardiac troponin biomarkers," *Sci. Rep.*, vol. 6, no. 1, pp. 1–10, Dec. 2016.

[35] X. Yu *et al.*, "A nanostructured microfluidic immunoassay platform for highly sensitive infectious pathogen detection," *Small*, vol. 13, no. 24, Jun. 2017, Art. no. 1700425.

[36] R. Ahmad, M.-S. Ahn, and Y.-B. Hahn, "ZnO nanorods array based field-effect transistor biosensor for phosphate detection," *J. Colloid Interface Sci.*, vol. 498, pp. 292–297, 2017.

[37] R. Ahmad *et al.*, "Highly efficient non-enzymatic glucose sensor based on CuO modified vertically-grown ZnO nanorods on electrode," *Sci. Rep.*, vol. 7, no. 1, pp. 1–10, Dec. 2017.

[38] R. Ahmad, N. Tripathy, M.-S. Ahn, and Y.-B. Hahn, "Solution process synthesis of high aspect ratio ZnO nanorods on electrode surface for sensitive electrochemical detection of uric acid," *Sci. Rep.*, vol. 7, no. 1, pp. 1–8, Jun. 2017.

[39] M. F. M. Fathil *et al.*, "Substrate-gate coupling in ZnO-FET biosensor for cardiac troponin I detection," *Sens. Actuators B, Chem.*, vol. 242, pp. 1142–1154, Apr. 2017.

[40] M. Fathollahzadeh *et al.*, "Immobilization of glucose oxidase on ZnO nanorods decorated electrolyte-gated field effect transistor for glucose detection," *J. Solid State Electrochem.*, vol. 22, no. 1, pp. 61–67, Jan. 2018.

[41] J.-H. Han, D. Lee, C. H. C. Chew, T. Kim, and J. J. Pak, "A multi-virus detectable microfluidic electrochemical immunosensor for simultaneous detection of H1N1, H5N1, and H7N9 virus using ZnO nanorods for sensitivity enhancement," *Sens. Actuators B, Chem.*, vol. 228, pp. 36–42, Jun. 2016.

[42] N. P. Shetti, S. D. Bukkitgar, K. R. Reddy, C. V. Reddy, and T. M. Aminabhavi, "ZnO-based nanostructured electrodes for electrochemical sensors and biosensors in biomedical applications," *Biosensors Bioelectron.*, vol. 141, Sep. 2019, Art. no. 111417.

[43] Y. Xia *et al.*, "Smartphone-based point-of-care microfluidic platform fabricated with a ZnO nanorod template for colorimetric virus detection," *ACS Sensors*, vol. 4, no. 12, pp. 3298–3307, Dec. 2019.

[44] B. Chakraborty, S. Ghosh, N. Das, and C. RoyChaudhuri, "Liquid gated ZnO nanorod FET sensor for ultrasensitive detection of hepatitis B surface antigen with vertical electrode configuration," *Biosensors Bioelectron.*, vol. 122, pp. 58–67, Dec. 2018.

[45] S. S. A. Karim, C.-F. Dee, B. Y. Majlis, and M. A. Mohamed, "Recent progress on fabrication of zinc oxide nanorod-based field effect transistor biosensors," *Sains Malaysiana*, vol. 48, no. 6, pp. 1301–1310, Jun. 2019.

[46] A. K. Assaifan, J. S. Lloyd, S. Samavat, D. Deganello, R. J. Stanton, and K. S. Teng, "Nanotextured surface on flexographic printed ZnO thin films for low-cost non-faradaic biosensors," *ACS Appl. Mater. Interfaces*, vol. 8, no. 49, pp. 33802–33810, Dec. 2016.

[47] M. Sasmal, T. K. Maiti, and T. K. Bhattacharyya, "Ultra-low level detection of L-histidine using solution-processed ZnO nanorod on flexible substrate," *IEEE Trans. Nanobiosci.*, vol. 14, no. 6, pp. 634–640, Sep. 2015.

[48] S. Lv, K. Zhang, L. Zhu, and D. Tang, "ZIF-8-assisted $NaYF_4$:Yb,Tm@ZnO converter with exonuclease III-powered DNA Walker for near-infrared light responsive biosensor," *Anal. Chem.*, vol. 92, no. 1, pp. 1470–1476, Jan. 2020.

[49] K. Sinha, R. Majumder, and C. D. Mukhopadhyay, *Advances in Bioprocess Engineering and Technology* (Lecture Notes in Bioengineering), 5th ed. Singapore: Springer, 2021, pp. 29–37.

[50] B. Chakraborty *et al.*, "Impact of surface defects in electron beam evaporated ZnO thin films on FET biosensing characteristics towards reliable PSA detection," *Appl. Surf. Sci.*, vol. 537, Jan. 2021, Art. no. 147895.

[51] R. Hoffman, *ZnO Thin-Fim Transistors*. Amsterdam, The Netherlands: Elsevier, 2006, pp. 415–442.

[52] P. R. Nair and M. A. Alam, "Performance limits of nanobiosensors," *Appl. Phys. Lett.*, vol. 88, no. 23, 2006, Art. no. 233120.

[53] *Serotonin ELISA*. [Online]. Available: https://eaglebio.com/product/serotonin-elisa-assay-kit/

[54] A. Murugesan *et al.*, "Serum serotonin levels in patients with epileptic seizures," *Epilepsia*, vol. 59, no. 6, pp. 91–97, 2018.

[55] J. Zhou, N. S. Xu, and Z. L. Wang, "Dissolving behavior and stability of ZnO wires in biofluids: A study on biodegradability and biocompatibility of ZnO nanostructures," *Adv. Mater.*, vol. 18, no. 18, pp. 2432–2435, 2006.

[56] F. Mollarasouli, S. Kurbanoglu, and S. A. Ozkan, "The role of electrochemical immunosensors in clinical analysis," *Biosensors*, vol. 9, no. 3, p. 86, Jul. 2019.

[57] K. Mahato, B. Purohit, K. Bhardwaj, A. Jaiswal, and P. Chandra, "Novel electrochemical biosensor for serotonin detection based on gold nanorattles decorated reduced graphene oxide in biological fluids and in vitro model," *Biosensors Bioelectron.*, vol. 142, Oct. 2019, Art. no. 111502.

[58] M. Kundys-Siedlecka, E. Bączyńska, and M. Jönsson-Niedziółka, "Electrochemical detection of dopamine and serotonin in the presence of interferences in a rotating droplet system," *Anal. Chem.*, vol. 91, no. 16, pp. 10908–10913, Aug. 2019.

[59] I. M. Apetrei and C. Apetrei, "Amperometric tyrosinase based biosensors for serotonin detection," *Romanian Biotechnol. Lett.*, vol. 18, no. 3, pp. 8253–8262, 2013.

[60] K. Mahato, A. Srivastava, and P. Chandra, "Paper based diagnostics for personalized health care: Emerging technologies and commercial aspects," *Biosensors Bioelectron.*, vol. 96, pp. 246–259, Oct. 2017.

[61] P. Chandra and R. Prakash, *Nanobiomaterial Engineering: Concepts and Their Applications in Biomedicine and Diagnostics*, 1st ed. London, U.K.: Springer, 2016, pp. 1–294.